# A DFT-Based Theoretical Study on the Photophysics of 4-Hydroxyacridine: Single-Water-Mediated Excited State Proton Transfer

**ARTICLE** *in* THE JOURNAL OF PHYSICAL CHEMISTRY A · FEBRUARY 2010

Impact Factor: 2.69 · DOI: 10.1021/jp909029c · Source: PubMed



**4 AUTHORS**, INCLUDING:

Bijan Kumar Paul
Indian Institute of Science Education and …
**72** PUBLICATIONS **895** CITATIONS
SEE PROFILE

Subrata Mahanta
National Institute of Advanced Industrial S…
**25** PUBLICATIONS **398** CITATIONS
SEE PROFILE

Rupashree Balia Singh
National Institute of Advanced Industrial S…
**27** PUBLICATIONS **419** CITATIONS
SEE PROFILE

# A DFT-Based Theoretical Study on the Photophysics of 4-Hydroxyacridine: Single-Water-Mediated Excited State Proton Transfer

**Bijan Kumar Paul, Subrata Mahanta, Rupashree Balia Singh, and Nikhil Guchhait***

*Department of Chemistry, University of Calcutta, 92 A. P. C. Road, Kolkata 700009, India*

*Received: September 18, 2009; Revised Manuscript Received: December 30, 2009*

Study of intra- and intermolecular hydrogen-bonding interaction and excited state proton transfer reaction has been carried out in 4-hydroxyacridine (4-HA) and its hydrated clusters theoretically. Density functional theory [B3LYP/6-311++G(d,p)] has been exploited to calculate structural parameters and relative energies of different conformers of 4-HA and its hydrates. The substantial impact of solvent reaction field on hydrogen-bond energies, conformational equilibrium, and tautomerization reaction in aqueous medium have been realized by employing Onsager and PCM reaction field methods, and the stability of the conformers of 4-HA is found to be profusely modulated by the electrostatic influence of the solvent. A deeper insight into the nature of H-bonding in 4-HA and its hydrated clusters has been achieved under the provision of natural bond orbital and atoms in molecule analysis. Elucidation of potential energy curves for proton transfer reaction reveals that an intrinsic and two-water-molecule-assisted proton transfer (PT) reaction in 4-HA is hindered by high energy barrier in the $S_1$ surface, whereas single-water-assisted PT reaction is practically rendered barrierless. At the same time, the appreciably high barrier height of the ground state potential energy curve in all the cases unambiguously rules out the possibility of ground state proton transfer reaction.

## 1. Introduction

Proton transfer (PT) reactions and hydrogen bonds in heterocycles play a vital role in many chemical and biological systems.[1−5] An interesting type of proton transfer in aqueous solution is one in which one or more solvent water molecules can mediate the process by serving as a bridge that connects the donor and acceptor sites. These water molecules stabilize the transition state and thereby substantially lower the classical energy barrier for proton transfer reaction. Such phenomenon has been postulated in the action of enzymes (e.g., carbonic acid anhydrase[6]) as well as in other tautomerization reactions.[7,8] The phenomenon of solvent-assisted tautomerization has grabbed attention over the years both from experimental and theoretical perspectives.[9−15] Simons and co-worker[16] have found that the activation energy barrier of formamide is lowered by 26.0 kcal/mol by adding simply one water molecule. Because of the light mass of the proton, quantum mechanical tunneling is very important in these reactions, and the shape of the potential energy surface (PES) has an influence on the tunneling probability. Truong and co-workers have calculated tunneling probabilities and rate constants for the double proton transfer in water-assisted tautomerization and found that the tunneling effect is very large, which lowers the barrier by about 4.60 kcal/mol.[17] Double proton transfer, quite naturally by virtue of its potential relevance to biological systems[6] and diagnosis of many chemical reactions,[7,8] has long been an active topic of research for theoreticians as well as experimentalists.[18−25] Recently, Li et al.[15] used HF, DFT, and CASSCF methods and showed that 8-hydorxyquinoline (8-HQ) can show more facile excited state proton transfer (ESPT) in the presence of a single water molecule compared to that in the absence of the same.

In the present study, we are interested in the proton transfer reaction in 4-hydroxyacridine (4-HA), a molecule very similar to 8-HQ and 7-hydroxy-1-indanone (7HIN).[16−18] The molecule acridine is an aza-polycyclic aromatic hydrocarbon found in the partial combustion of fossils fuels and tobacco and also detected in motor vehicle exhaust emissions, cigarette smoke, shale oil, coal tar, and coal liquefaction products.[26] Our target molecule, 4-HA, is a substituted product of the parent molecule, acridine. A detailed photophysical study and characterization of 4-HA is demanding due to its wide range of potential applications as a good chelating agent in analytical chemistry. The cyclopalladated complex of 4-HA is known to have anticancer activity,[27] and metal complexes of 4-HA are known to serve as the intercalators for DNA,[27] etc. Very recently, we have reported a spectral study of 4-HA[24] and shown that photophysical properties are reasonably distinct from other studied related molecules having a six-membered intramolecular hydrogen-bond (IMHB) ring between the proton donor and acceptor systems.[11−13] The molecule 4-HA, having a five-membered IMHB ring imparts a strain to the hydrogen-bonded site, and hence, the hydrogen bond is weak in nature. However, the most interesting observation is that the molecule 4-HA shows a solvent-water-mediated ESPT reaction.[24] The principal objectives of the present work is thus to carry out a detailed theoretical analysis of the photophysics of 4-HA with particular attention being inclined along a solvent-water-assisted ESPT reaction. Density functional theory has been implemented to calculate the ground-state structural parameters, relative energies of different conformers of 4-HA, and tautomers of hydrates of 4-HA. Atoms in molecule (AIM) and natural bond orbital (NBO) analysis have been performed to get a better understanding of the hydrogen-bonding interaction. The ground- and excited-state potential energy surfaces (PESs) have been evaluated along the proton transfer coordinate for the bare molecule and its hydrated clusters to ascertain the feasibility of the process. Several transition state structures proposed for the tautomerization processes have also been examined carefully.

* To whom correspondence should be addressed. Fax: +91 33 2351 9755. E-mail: nguchhait@yahoo.com.

10.1021/jp909029c 
Published on Web 02/01/2010

## 2. Computational Methods

All calculations have been performed with the Gaussian 03 suit of program using the density functional theoretical (DFT) method with the B3LYP hybrid functional.[28] In our calculation, the 6-311++G(d,p) basis set is stressed because this basis set is of triple-$\xi$ quality[28,30] for valence electrons with diffuse functions which are useful in calculations for anions and structures with lone pair electrons.[31,32] [Calculation with the other basis sets 6-31G(d,p) and 6-31++G(d,p) have also been performed but are not mentioned in this paper. A comparison of results of different basis sets reflects that the most crucial achievement of H-bond energy comes with this basis set. This observation gracefully complies with other reports[29]]. We have exploited the 6-311++G(d,p) basis set for calculation considering the necessity of diffuse functions for full characterization of the hydrogen-bond interaction.[28−32]

The geometrical constraints were not imposed in equilibrium geometry calculations and in the transition state structure optimizations. Vibrational frequency analyses were carried out for the optimized structures in order to assess the nature of stationary points and to obtain zero point vibration energy (ZPE). The characteristics of local minima and transition states (TS) were verified by establishing that matrices of energy second derivatives (Hessian) have either zero or one imaginary frequency.[28] Further characterization of the TS was achieved from calculation of the intrinsic reaction coordinate (IRC).[29]

For solution-phase calculation, self-consistent field calculation was exploited to optimize the structure of different forms of 4-HA as well as the transition states. The SCRF theory was used to optimize the structures and to calculate the energies of 4-HA and 4-HA−water complex at the given value of dielectric constants, i.e., $\varepsilon = 78.39$ for water. Frequencies were calculated for both the ground and transition states. In the Onsager model,[33] the radius of the solute molecular system was calculated from the molecular volume for the structure optimized in the gaseous phase. In the polarizable continuum model (PCM),[34,35] the solute, treated quantum chemically, is placed in a cavity surrounded by the solvent. The latter is considered as a continuum characterized by its bulk properties, such as a dielectric constant and polarity.

Stabilization energies ($\Delta E_{stab}$) of 4-hydroxyacridine−water (4HA−$H_2O$) complex have been calculated as follows:

$$\Delta E_{stab} = E_{complex} - (E_{4\text{-HA}} + E_{water})$$

Here $E_{complex}$, $E_{4\text{-HA}}$, and $E_{water}$ are the energies of 4-HA−water complex, 4-HA, and one water molecule, respectively. The stabilization energy was corrected for basis set superposition error (BSSE) using the method of Boys and Bernardi.[36] The BSSE was corrected by the Boys and Bernardi counterpoise correction scheme as follows:

$$\text{BSSE} = 2[E_m(\text{M}) + E_m(\text{M}')] - [E_m(\text{M}) + E_d(\text{M}')]$$

where $E_m(\text{M})$ and $E_d(\text{M}')$ are the energies of the monomer in its own basis set and in the basis set of dimer, respectively, and M and M′ denote the optimized geometry of monomer and in the optimized adduct, respectively. So corrected stabilization energy of the complex is

$$\Delta E_{stab}(\text{corrected}) = \Delta E_{stab} + \text{BSSE}$$

Intrinsic reaction coordinate (IRC)[37,38] calculations in which the imaginary mode for the transition state is followed in both the forward and reverse directions were used to connect the transition states to their respective minima. The NBO[39,40] second-order perturbation stabilization energy ($\Delta E_2$) is calculated as follows:

$$\Delta E_2 = \Delta E_{ij}^{(2)} = \frac{|\langle \Phi_i | \hat{F} | \Phi_j \rangle|^2}{(\varepsilon_i - \varepsilon_j)}$$

where $\hat{F}$ is the Fock operator and $\varepsilon_i$ and $\varepsilon_j$ correspond to the energy eigenvalues of the donor molecular orbital $\Phi_i$ and the acceptor molecular orbital $\Phi_j$, respectively.

For the excited states, the TDDFT[42,43] method was used to calculate the vertical excitation energy with the same B3LYP parametrization and 6-311++G(d,p) basis set. The possibility of ground-state intramolecular proton transfer (GSIPT) was explored on the potential energy curve (PEC) constructed by observing variation of energy as a function of $O_{17}-H_{24}$ distance (Schemes 1−3). Information regarding the ESIPT mechanism was obtained by constructing the Franck−Condon curves by adding the TDDFT/6-311++G(d,p) vertical excitation energies to the corresponding GSIPT curves. Such methods have successfully been implemented to evaluate the PESs for the excited state proton transfer reaction.[24,44]

## 3. Results and Discussions

**3.1. Bare 4-HA.** ***3.1.1. Geometry, Energy and Structural Parameters.*** The optimized structural parameters of different conformers of 4-HA (Scheme 1) are presented in Table 1. The symmetry of the molecular structures **I**−**III** lie in the $C_s$ point group and the transition state **TS1** belongs to the $C_1$ point group. This advocates the planarity of all structures **I**−**III** in the gaseous phase; hence, no symmetry constraint was imposed during calculations. With a view to the proton transfer (PT) reaction, the mostly concerned parameters at the IMHB site in 4-HA are the $O_{17}-H_{24}$, $N_7-H_{24}$, and $O_{17}-N_7$ distances (Scheme 1). The calculated O−H bond distance is 0.964 Å in conformer **II**, and this distance lengthens a little on going to conformer **I** along with a little shortening of the $O_{17}-N_7$ distance (Table 1). As for the proton transfer process, we observe enlargement of the $O_{17}-H_{24}$ bond and shortening of the $N_7-H_{24}$ distance on passing from **I** to **III**. The distance between the acceptor nitrogen atom ($N_7$) and the labile hydrogen ($H_{24}$) in **I**, as well as between the donor oxygen atom ($O_{17}$) and $H_{24}$ in **III** are both close to 2.0 Å, indicating the possibility of IMHB in **I** and **III** (Table 1). As far as the angular changes are concerned, the angle $\angle C_4-O_{17}-H_{24}$ shortens by ∼3° and $\angle C_5-N_7-H_{24}$ and $\angle N_7-H_{24}-O_{17}$ exhibit an appreciable increase on passing from **II** to **I**. On proton transfer, $\angle N_7-H_{24}-O_{17}$ decreases by ∼6° and $\angle C_4-O_{17}-H_{24}$ decreases considerably from **I** to **III** (Table 1).

The influence on the geometry of the molecule exerted by the introduction of the solvent reaction field is noteworthy. It is seen that the $O_{17}-H_{24}$ bond elongates by 0.006 Å from gaseous phase to aqueous medium for conformer **I**, but in case of conformer **III**, the increase is by 0.207 Å. For $N_7-H_{24}$ distance, passing to aqueous solution from gaseous phase results in an increment of 0.116 Å for conformer **I**, while for conformer **III** the increment is very small, only 0.002 Å. In the case of the $O_{17}-N_7$ distance, which is a very crucial parameter for the conversion of **I** to **III**, it is increased by 0.052 Å in conformer **I**, but in **III** the increment is 0.094 Å on going from gaseous to

**SCHEME 1: Different Conformers of 4-HA and Its Proton Transfer Reaction Scheme**

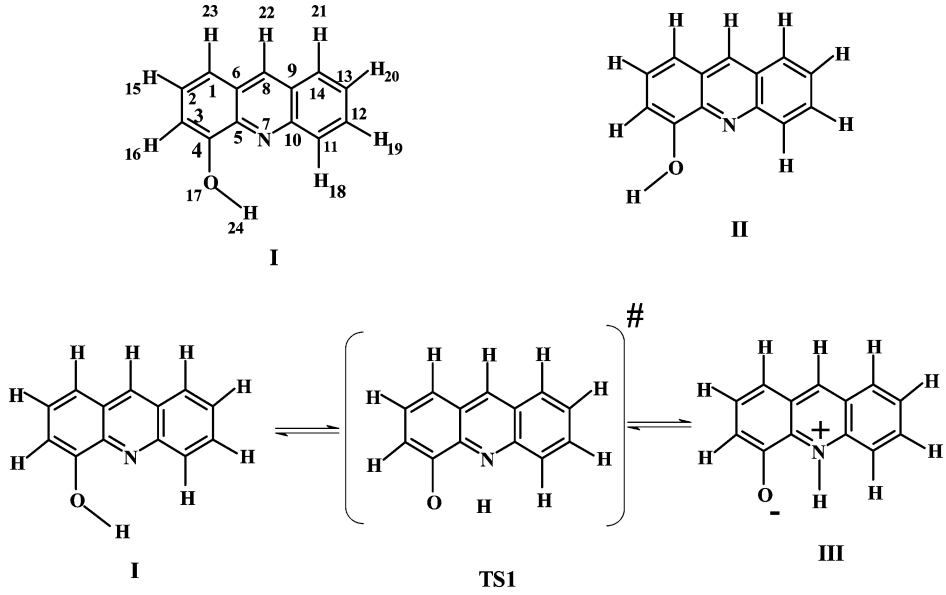


**SCHEME 2: Proton Transfer Reaction Scheme for Monohydrates of 4-HA**

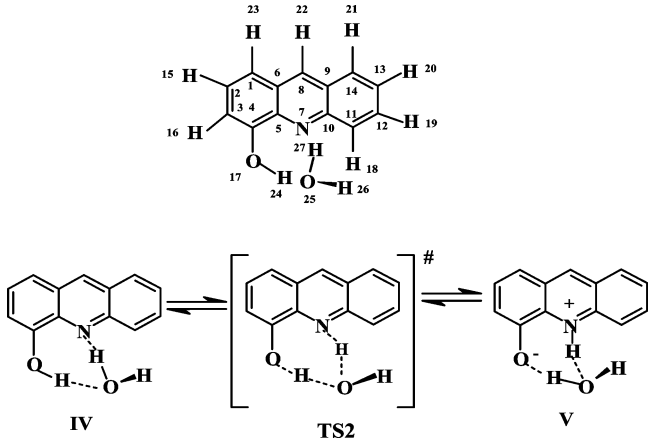


aqueous phase. From Table 1 it is obvious that all the atoms, especially $C_4$, $C_5$, $N_7$, $O_{17}$, and $H_{24}$ in 4-HA, are all on the same plane. The angle $\angle O_{17}-H_{24}-N_7$ of conformer **I** is 117.449° in the gaseous phase and 112.365° in the aqueous phase. In conformer **III**, the $\angle O_{17}-H_{24}-N_7$ angle is decreased from 110.825° to 103.473° from gaseous to aqueous phase. So the change of $\angle O_{17}-H_{24}-N_7$ angle in conformer **III** is greater than that in conformer **I** as a result of the introduction of the solvent reaction field. The most remarkable change in angle from conformer **I** to **III** is in case of $\angle C_4-O_{17}-H_{24}$ angle; this change is remarkably larger in comparison to other angular changes of 4-HA.

***3.1.2. Relative Stability of Different Conformers.*** Calculations predict conformer **I** to be the most stable form in the gaseous phase, while conformer **III** is the least stable one (~13.0 kcal/mol higher with respect to **I**; Table 2). This is a positive indication toward the extra stability gained by the IMHB in conformer **I** of 4-HA. The influence of solvent on the stability of different conformers is also portrayed in Table 2. It is interesting to see that incorporation of a solvent effect (using the PCM in water) has remarkable influence on the stability of conformer **III** relative to **I** (enhanced stability of conformer **III**,

**SCHEME 3: Proton Transfer Reaction Scheme for Dihydrates of 4-HA**

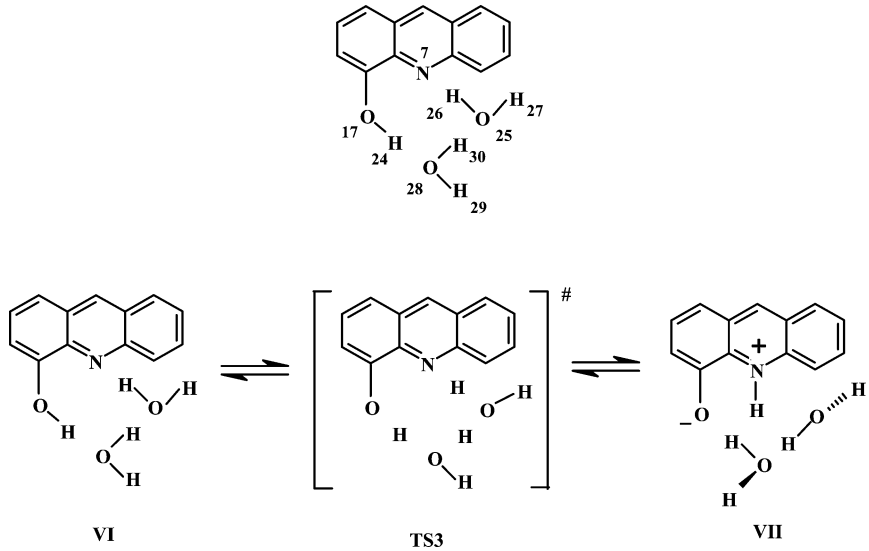

**TABLE 1: Selected Optimized Geometries for Rotamers and Tautomers of 4-HA in Gaseous Phase and in Solvent Water[a]**

| | I | | II | | III | |
|---|---|---|---|---|---|---|
| structural parameters | A | B | A | B | A | B |
| | | | Bond Length (Å) | | | |
| $N_7-H_{24}$ | 2.077 | 2.193 | 3.650 | 3.682 | 1.031 | 1.033 |
| $O_{17}-H_{24}$ | 0.975 | 0.981 | 0.964 | 0.984 | 2.064 | 2.271 |
| $O_{17}-C_4$ | 1.350 | 1.357 | 1.357 | 1.358 | 1.259 | 1.280 |
| $O_{17}-N_7$ | 2.670 | 2.722 | 2.694 | 2.704 | 2.611 | 2.705 |
| | | | Bond Angle (deg) | | | |
| $\angle C_4-O_{17}-H_{24}$ | 105.775 | 108.928 | 109.176 | 110.112 | 86.309 | 84.287 |
| $\angle C_5-N_7-H_{24}$ | 82.232 | 81.864 | 59.925 | 59.824 | 111.047 | 115.721 |
| $\angle N_7-H_{24}-O_{17}$ | 117.449 | 112.365 | 6.122 | 5.448 | 110.825 | 103.473 |
| | | | Dihedral Angle (deg) | | | |
| $\angle C_6-C_5-C_4-O_{17}$ | 180.00 | 180.00 | 180.00 | 180.00 | 180.00 | 179.81 |
| $\angle C_5-C_4-O_{17}-H_{24}$ | 0.00 | 0.00 | 180.00 | 180.00 | 0.00 | 0.27 |
| $\angle C_9-C_{10}-N_7-H_{24}$ | 180.00 | 180.00 | 0.000 | 0.00 | −180.00 | −179.86 |

[a] A, B3LYP/6-311++G**; B, PCM/B3LYP/6-311++G**.

**TABLE 2: Calculated Energy Relative to I ($\Delta E$ in kcal/mol) for Rotamers and Tautomers of 4-Hydroxyacridine in the Gaseous Phase and Aqueous Phase Including ZPE Correction**

| | I | | II | | III | |
|---|---|---|---|---|---|---|
| functional and basis set | $\Delta E$ | $\mu$ (D) | $\Delta E$ | $\mu$ (D) | $\Delta E$ | $\mu$ (D) |
| B3LYP/6-311++G** | 0.0 | 2.986 | 7.754 | 2.037 | 13.768 | 7.087 |
| B3LYP/6-311++G**[a] | 0.0 | 4.266 | 7.966 | 3.482 | −7.198 | 11.689 |
| B3LYP/6-311++G**[b] | 0.0 | 4.590 | 8.397 | 2.908 | 10.726 | 10.644 |

[a] Using PCM, at the B3LYP/6-311++G**level. [b] According to the Onsager solvent reaction field.

$E_{III} = -7.198$ kcal/mol) and, at the same time, only negligible influence on the energy of conformer **II** (Table 2). These observations are in line with usual expectations that polar solvent water will preferably stabilize conformer **III** with a higher dipole moment, so that SCRF calculations predict conformer **III** to be favored over **I** in aqueous medium. Table 2 also highlights the results according to the Onsager solvent reaction filed, which does not predict structure **III** to be of lowest energy in solvent water as opposed to normal arguments and results of the PCM. The failure of the Onsager model to predict the energy stability trend could be due to the assumption of a spherical cavity. The spherical cavity might be inadequate given the planarity of the molecule; additionally, the Onsager approach requires the electric dipole to be located at the cavity center, which is not true in most cases.[29]

***3.1.3. Mulliken Charge and Dipole Moment Analysis.*** The stability of different conformers of 4-HA are sensitive toward the action of the solvent reaction field, and it is evident that the charge distribution and dipole moments (Table 2) play important roles in determining the solute−solvent interactions in the present case. We have specially noted the Mulliken charge (MC) distribution over the $N_7$, $O_{17}$, and $H_{24}$ atoms for different conformers of 4-HA (Table 3). Interestingly the process of proton transfer (PT) (**I→III**) involves a more pronounced variation of MC on $N_7$ and $O_{17}$ rather than $H_{24}$, such as the numerical magnitudes of changes at $N_7$ (decrease of negative charge density) and $O_{17}$ (increase of negative charge density) are 0.292 and −0.220, respectively.

Table 3 also reflects that the action of the solvent [water in the present case; PCM, B3LYP/6-311++G(d,p) level] reaction field profusely modifies the MC distribution over the atoms. Such significant effect of solvent on charge distribution naturally implies that the solvent should influence the internuclear distances also (see section 3.1.1 and Table 1). The lengthening of the $N_7\cdots H_{24}$ distance (in conformer **I**) in aqueous solution compared to that in the gaseous phase may thus be attributed to the lowering of energy due to the dipole−dipole interaction between polar solvent and solute molecules which may suffice to lose considerably the intramolecular forces in solution. Thus, the exertion of the polar solvent reaction field leads to weakening of the hydrogen bond.[29,45]

The calculated dipole moments for conformers **I** to **III** are summarized in Table 2. The differences in dipole moments are found to be more pronounced in aqueous solution than in the gaseous phase. The much higher dipole moment of **III** compared to that of **I** and **II** ensures that polar solvent exerts a greater effect on structure **III**, making it preferable to other conformers in solution. The direction of the dipole moment vector (Figure 1) is also important, as it determines the functional groups of 4-HA with which the solvent molecules interact.

***3.1.4. Excited State Potential Energy Surface.*** Since experiments have revealed conclusive evidence of water-mediated proton transfer in 4-HA,[24] analysis of the potential energy surfaces (PESs) both in the ground and excited states will play a vital role in deciphering the photophysics of 4-HA with particular attention to the ESPT process. This has driven us to construct the potential energy curve (PEC) for the PT reaction (Figure 2), which has been done according to the "*distinguished coordinate approach,*", i.e., by specifying a reaction coordinate (RC) along which energy change is observed.[18−20,23,44] In this case, the RC is the coordinate along which the proton undergoes translocation from $O_{17}$ to $N_7$, i.e., elongation of $O_{17}-H_{24}$ bond

**TABLE 3: Mulliken Charges at $N_7$, $O_{17}$, and Labile $H_{24}$ Atom of 4-HA**

| | I | | | II | | | III | | |
|---|---|---|---|---|---|---|---|---|---|
| functional and basis set | N | O | H | N | O | H | N | O | H |
| B3LYP/6-311++G** | −0.090 | −0.220 | 0.300 | −0.183 | −0.192 | 0.266 | 0.202 | −0.440 | 0.343 |
| B3LYP/6-311++G**[a] | −0.037 | −0.305 | 0.359 | −0.022 | −0.301 | 0.350 | 0.136 | −0.634 | 0.405 |

[a] Using PCM, at the B3LYP/6-311++G** level.

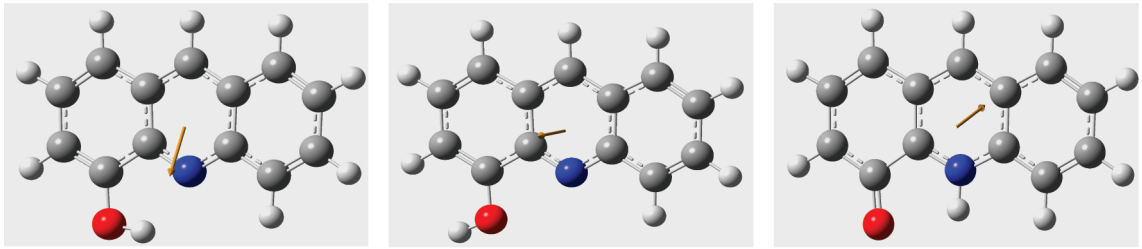

I II III

**Figure 1.** Dipole derivative unit vector $\vec{\mu}$ direction for the structures **I**, **II**, and **III** (obtained from calculation at the DFT//B3LYP/6-311++G(d,p) level).

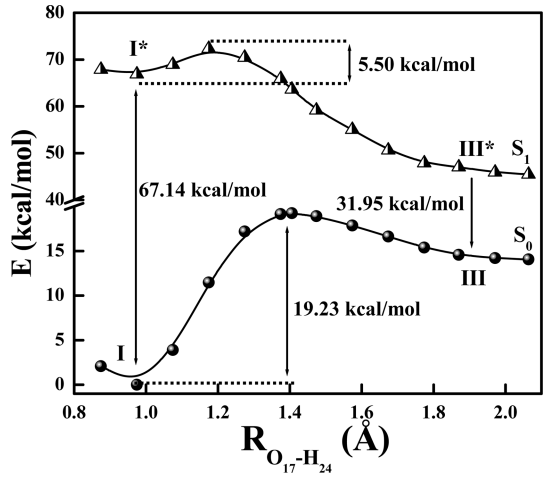


**Figure 2.** Potential energy curves for proton transfer reaction at the ground and first excited states of 4-HA using B3LYP/6-311++G(d,p) for the ground state and TD-B3LYP/6-311++G(d,p) for the excited state.

length of 4-HA for transformation **I**→**III**. The high barrier height at the ground state intramolecular proton transfer (GSIPT) curve (Figure 2) unanimously puts forward the nonviability of a GSIPT process (high barrier height of 19.23 kcal/mol, and for the reverse process, **III**→**I**, the barrier height is 2.62 kcal/mol). So conformer **I** constitutes the global minimum on the $S_0$ surface, and the existence of **III** on the $S_0$ surface is completely ruled out, since it is a high-energy conformer. Also as seen in Figure 2, the $S_1$ surface presents an asymmetric double-well-type potential along the RC with two minima corresponding to **I*** and **III*** forms. In the first excited state ($S_1$) the conversion **I**→**III** has to proceed through a barrier of 5.5 kcal/mol, which is not in line with other normal cases of ESIPT reaction, where it proceeds through an essentially barrierless surface. This result suggests that an intrinsic ESIPT in 4-HA encounters some definite energy barrier (5.5 kcal/mol is not an appreciably high barrier though). This result may be invoked to stand in complement of the experimental finding, i.e., inoperativeness of ESIPT in solvents other than water.[24]

**3.2. 4-HA−Water Monohydrate (Water-Assisted Tautomerization).** ***3.2.1. Structures, Energies, and Charges.*** In this section, we take into account the stability of tautomers of 4-HA by adding a single water molecule to 4-HA. Structures of different tautomers of the monohydrated complex (4-HA−$H_2O$) are presented in Scheme 2 and selected optimized geometry parameters are given in Table 4a. Table 4b puts light on the modifications in the stability of the structures coming from addition of one water molecule. Table 4b also reflects the substantial impact of the solvent reaction field on the stability of the conformers. Changes in the structural parameters brought

**TABLE 4: (a) Selected Optimized Geometry Parameters of Tautomers and Transition State for Tautomerization of 4-HA Complexed with One Water Molecule in the Gaseous Phase at the DFT/B3LYP/6-311++G** Level and (b) Energies and Dipole Moments ($\mu$/D) of Hydrated Clusters of 4-HA (i.e., Structures IV, V, and TS2) in Gaseous Phase and in Solvent Water (Including ZPE Correction)**

(a) Selected Optimized Geometry Parameters of Tautomers Transition State for Tautomerization

| parameters | IV | V | TS1 |
|---|---|---|---|
| | Bond Length (Å) | | |
| $N_7-H_{27}$ | 1.841 | 1.037 | 1.175 |
| $N_7-C_5$ | 1.345 | 1.352 | 1.353 |
| $O_{17}-H_{24}$ | 0.981 | 1.674 | 1.193 |
| $O_{17}-N_7$ | 2.862 | 2.764 | 2.501 |
| $O_{25}-H_{24}$ | 1.784 | 0.995 | 1.215 |
| $O_{25}-H_{27}$ | 0.985 | 1.794 | 1.326 |
| | Bond Angle (deg) | | |
| $\angle C_5-N_7-H_{27}$ | 125.466 | 117.774 | 118.120 |
| $\angle O_{17}-H_{24}-O_{25}$ | 176.091 | 157.959 | 169.664 |
| $\angle N_7-H_{27}-O_{25}$ | 156.705 | 175.513 | 166.273 |
| $\angle H_{24}-O_{25}-H_{27}$ | 76.637 | 75.902 | 82.896 |
| $\angle H_{27}-O_{25}-H_{26}$ | 107.032 | 128.930 | 117.783 |
| | Dihedral Angle (deg) | | |
| $\angle C_9-C_{10}-N_7-H_{27}$ | −174.523 | −178.741 | −177.281 |
| $\angle O_{17}-H_{24}-O_{25}-H_{27}$ | −111.459 | −4.429 | 1.713 |
| $\angle N_7-H_{27}-O_{25}-H_{24}$ | −10.069 | −36.182 | −15.114 |

(b) Energies and Dipole Moments ($\mu$/D) of Hydrated Clusters of 4-HA[a]

| | IV | | V | | TS2 | |
|---|---|---|---|---|---|---|
| level | $\Delta E$ | $\mu$ | $\Delta E$ | $\mu$ | $\Delta E$ | $\mu$ |
| B3LYP/6-311++G** | 0.0 | 4.289 | 7.024 | 8.983 | 4.504 | 5.827 |
| B3LYP/6-311++G**[b] | 0.0 | 6.363 | 5.048 | 10.664 | 2.353 | 10.664 |
| B3LYP/6-311++G**[c] | 0.0 | 4.289 | 5.215 | 9.705 | 7.764 | 7.912 |

[a] Energies ($\Delta E$ in kcal/mol) are relative to structure **IV**. [b] Using PCM, at the B3LYP/6-311++G** level. [c] According to the Onsager solvent reaction field.

about by the incorporation of one water molecule are evident from analysis of the parameters given (Table 4a) but what is required to be particularly highlighted here is the two intermolecular H-bonds ($I_{er}$MHB) in 4-HA−$H_2O$, viz., $O_{17}-H_{24}\cdots O_{25}$ and $O_{25}-H_{27}\cdots N_7$ in **IV** and $O_{17}\cdots H_{24}-O_{25}$ and $O_{25}\cdots H_{27}-N_7$ in **V** (Scheme 2). Here the water molecule plays the role of a bridge between $H_{24}$ and $N_7$ of the 4-HA−$H_2O$ cluster. This is an indication of the cooperative character of two hydrogen bonds in conformers **IV** and **V**, i.e., the interaction in which a molecule is participating simultaneously as a donor and an acceptor.[29,39,45] Upon formation of the H-bond, the $O_{17}-H_{24}$ length in **IV** and the $N_7-H_{27}$ length in **V** elongates (Tables 1 and 4a). Also the two O−H bond lengths of the water molecule are equal neither

in structure **IV** nor in **V** (Table 4a). The O−H length involved in $I_{er}$MHB is longer. Such geometrical condition justifies the presence of $I_{er}$MBH in **IV** and **V**; at the same time, the inequality of the $N_7\cdots H_{27}$ and $H_{24}\cdots O_{25}$ distances point toward the differential energies of the two H-bonds present in **IV** and **V**.

In order to follow the effect of solvent on the geometries of **IV**, **V**, and **TS2**, these structures have been optimized in medium with $\varepsilon = 78.39$, i.e., water. For aqueous solution, the $N_7-H_{27}$ distance in **IV** is 0.034 Å shorter than the corresponding value in the gaseous phase, while the $O_{25}-H_{24}$ distance is 0.015 Å longer. The partial charges on the $O_{17}$, $N_7$, and $O_{25}$ atoms in **IV** according to Mulliken population analysis are −0.393, 0.061, and −0.627 in the gaseous phase and the values change to −0.447, 0.010, and −0.684, respectively, in aqueous medium ($\varepsilon = 78.39$). The Mulliken charges in aqueous solution have been calculated with B3LYP/6-311++G(d,p) using PCM. Weak hydrogen bonds are primarily electrostatic in nature. The higher negative charge on $O_{17}$ in the solution makes the attractive electrostatic interactions with the H atom of the extra water molecule stronger than in the gaseous phase. The $N_7-H_{27}$ distance becomes smaller, while the smaller positive charge on $N_7$ makes the attractive interactions in the solution greater than that in the gaseous phase and the $O_{25}-H_{24}$ distance is larger. Thus, the changes of partial charges on atoms and H-bond lengths as a result of switching the medium seem to correlate well with each other.

For structure **V**, the $O_{17}-H_{24}$ and $N_7-H_{27}$ distances decrease by 0.025 and 0.003 Å on passing from gaseous phase to the aqueous medium. The partial Mulliken charges on $N_7$, $O_{17}$, and $O_{25}$ in the gaseous phase are respectively 0.079, −0.478, and −0.612, and in aqueous medium ($\varepsilon = 78.39$) for same atoms the values are 0.091, −0.631 and −0.661, respectively. Thus, the higher electronic density on $O_{17}$ atom makes the hydrogen bond in structure **V** stronger and shorter in aqueous medium relative to that in the gaseous phase. As for **TS2** also, moving from gaseous phase to aqueous solution exerts noticeable changes on its geometry. The $H_{24}-O_{25}$ and $O_{25}-H_{27}$ distances increase by 0.002 and 0.044 Å, respectively, with a simultaneous decrease of $O_{17}-H_{24}$ and $N_7-H_{27}$ distances by 0.0561 and 0.0234 Å, respectively. Such changes in the hydrogen-bond lengths result in the separation of partial charges of **TS2** state and hence increase the dipole moment (Table 4b), making it more polar in a polar solvent (water) compared to that in the gaseous phase.

***3.2.2. NBO and AIM Analysis.*** The analysis of NBO developed by Weinhold[39] to study orbital interactions within any pair of interacting atoms has become one of the strongest tools available to date to evaluate intramolecular interactions such as hydrogen bonds. The NBO analysis transfers the delocalized MOs into the localized ones. The interaction between filled and antibonding orbitals represents the deviation of the molecule from the Lewis structure and can be used as a measure of the delocalization due to IMHBs. In the present program we have studied IMHBs in conformers **I** and **III** and $I_{er}$MHBs in **IV** and **V** under the provision of NBO analysis in order to gather a deeper insight into their nature and outcome.

The results of NBO analysis for conformers **I** and **III** are compiled in Table 5a. Emphasis has been given to the contributions involving the lone electron pairs of nitrogen and oxygen atoms. The delocalization interactions are found to be especially sizable for the $\pi$ system and for the lone pairs of nitrogen and oxygen. Table 5a clearly dictates that in **I** the charge transfer interactions from the lone pairs of electron donors (N and O) are directed mainly to the antibonding orbitals

**TABLE 5: (a) Second-Order Perturbation Energies $E_{i,j}^{(2)}$ (kcal/mol)[a] and (b) NBO Analysis (B3LYP/6-311++G(d,p)) of Complexes IV−V: the Nature of Donor Orbitals $\phi_i$, Acceptor Orbitals $\phi_j$, and the Second-Order Perturbation Energies $\Delta E_{ij}^{(2)}$ in kcal/mol**

(a) Second-Order Perturbation Energies

| donor NBO ($i$) → | acceptor NBO ($j$) | energy $E_{i,j}^{(2)}$ I | III |
|---|---|---|---|
| LP($N_7$) | BD*($C_5-C_6$) | 10.11 (0.04250) | − |
| LP($N_7$) | BD*($C_9-C_{10}$) | 9.64 (0.04410) | − |
| LP($N_7$) | BD*($O_{17}-H_{24}$) | 4.19 (0.02222) | − |
| LP($O_{17}$) | BD*($C_4-C_5$) | 5.64 (0.04295) | 17.43 (0.06902) |
| LP($O_{17}$) | BD*($C_3-C_4$) | 33.17 (0.28939) | 15.47 (0.04472) |
| LP($O_{17}$) | BD*($N_7-H_{24}$) | − | 4.33 (0.04752) |

(b) NBO Analysis (B3LYP/6-311++G(d,p)) of Complexes **IV**−**V**

| conformer | $\phi_i \rightarrow \phi_j$ | $\Delta E_{ij}^{(2)}$ |
|---|---|---|
| **IV** | LP($N_7$)→BD*($O_{25}-H_{27}$) | 16.99 |
| | LP1/LP2 ($O_{25}$)→BD*($O_{17}-H_{24}$) | 0.32/16.17 |
| **IV**[b] | LP($N_7$)→BD*($O_{25}-H_{27}$) | 15.79 |
| | LP1/LP2($O_{25}$)→BD*($O_{17}-H_{24}$) | 0.34/17.57 |
| **V** | LP1/LP2 ($O_{17}$)→BD*($O_{25}-H_{24}$) | 7.47/17.7 |
| | LP1/LP2 ($O_{25}$)→BD*($N_7-H_{27}$) | 0.45/17.55 |
| **V**[b] | LP1/LP2 ($O_{17}$)→BD*($O_{25}-H_{24}$) | 6.21/17.64 |
| | LP1/LP2 ($O_{25}$)→BD*($N_7-H_{27}$) | 0.33/15.1 |

[a] Numerical values in the parentheses indicate the occupation numbers of the corresponding antibonding orbitals, calculated at the DFT/B3LYP/6-311++G(d,p) level. [b] Using PCM at the B3LYP/6-311++G** level.

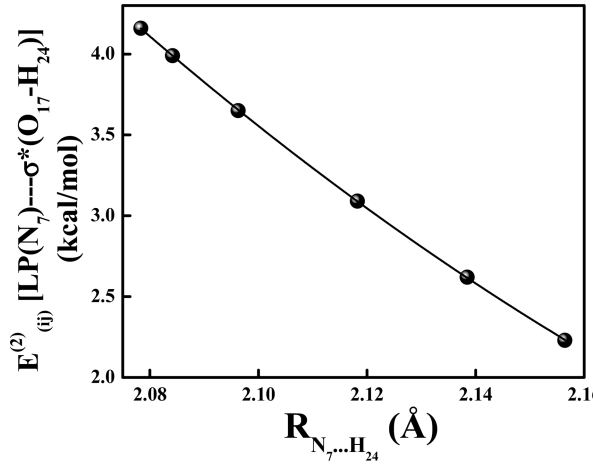


**Figure 3.** LP($N_7$)→$\sigma$*($O_{17}-H_{24}$) hyperconjugative interaction energy as a function of $N_7\cdots H_{24}$ IMHB distance of conformer **I** of 4-HA as obtained from NBO analysis in a relaxed scan performed at the DFT//B3LYP/6-311++G(d,p) level.

on the remote part of the molecule. In the case of structure **III** also, similar interactions are present to advocate for the IMHB leading to the formation of a five-member quasicycle.[29] Figure 3 depicts that the hyperconjugative stabilization interaction between $N_7$ lone pair and the $\sigma$*($O_{17}-H_{24}$) orbital is sharply diminished with elongation of the $N_7\cdots H_{24}$ IMHB, justifying the presence of IMHB in the five-member quasicycle. Similarly, the presence of $I_{er}$MHB in **IV** and **V** are confirmed within the NBO framework, as revealed by the data summarized in Table 5b (also the unequal strength of the two $I_{er}$MHBs: $N_7\cdots H_{27}$ and $O_{25}\cdots H_{24}$ in **IV** and $H_{27}\cdots O_{25}$ and $H_{24}\cdots O_{17}$ in **V** are predicted). The steep fall of the LP($O_{25}$)→$\sigma$*($O_{17}-H_{24}$) and LP($N_7$)→$\sigma$*($O_{25}-H_{27}$) hyperconjugative interaction energy for **IV** as a function of $O_{25}\cdots H_{24}$ and $N_7\cdots H_{27}$ distances, respec-

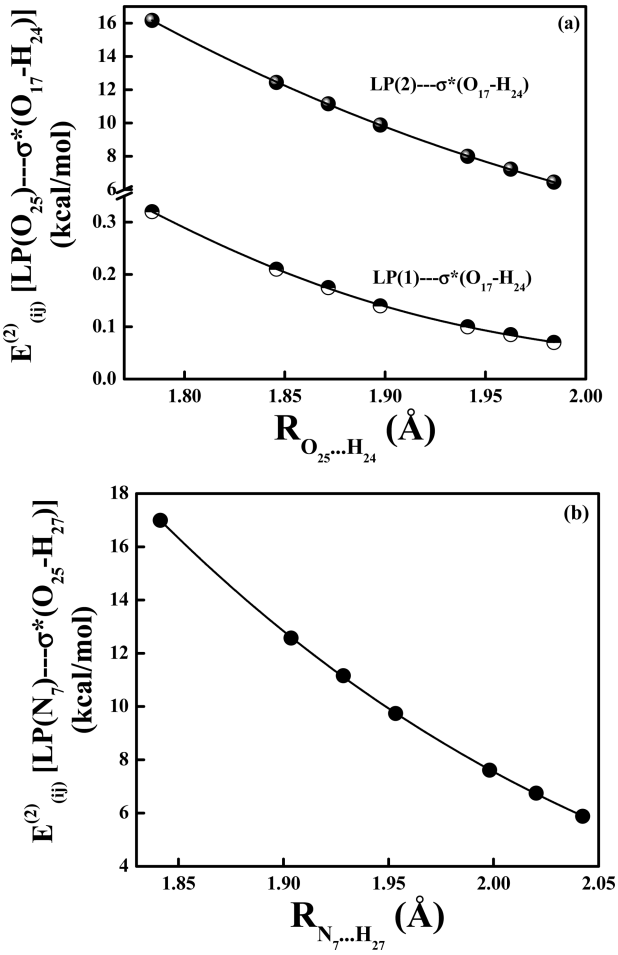


**Figure 4.** (a) LP($O_{25}$)→$\sigma^*$($O_{17}$−$H_{24}$) and (b) LP($N_7$)→$\sigma^*$($O_{25}$−$H_{27}$) hyperconjugative interaction energy as a function of $O_{25}\cdots H_{24}$ and $N_7\cdots H_{27}$ distances, respectively, of conformer **IV** of monohydrated cluster of 4-HA as obtained from NBO analysis in a relaxed scan performed at the DFT//B3LYP/6-311++G(d,p) level.

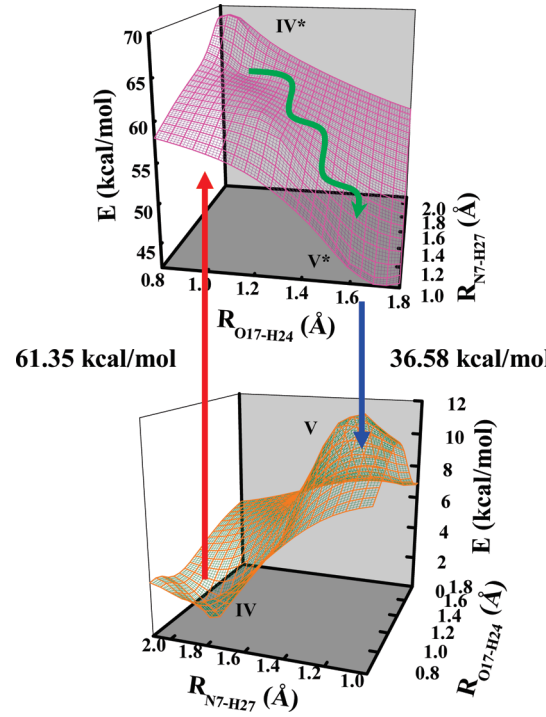


**Figure 5.** Three-dimensional potential energy surface for water-assisted proton transfer reaction in the monohydrated cluster of 4-hydroxyacridine (4-HA−$H_2O$).

tively (Figure 4), is evidence for the appreciable strength of the $I_{er}$MHBs present.

Again the formation of IMHB in **I** and **III** has further been explored within the AIM framework. The AIM method provides a means of mapping topological properties of the electron density to the Lewis structure representation of molecules.[41] The nature of bonding between atoms can be characterized by the value of $\rho(r)$ and the sign of the Laplacian $\nabla^2\rho(r)$ of the electron density at the bond critical point (BCP). Large $\rho(r)$ values together with negative $\nabla^2\rho(r)$ values represent shared interactions, characteristic of covalent bonds. In contrast, low $\rho(r)$ values along with positive $\nabla^2\rho(r)$ values are indicative of closed-shell interactions typically found in ionic bonds and H-bonds as well as in van der Waals interactions. Among those criteria to establish H-bond proposed by Koch and Popelier, "there is a BCP for the H···Y contact", "the value of $\rho(r)$ at BCP of H···Y lies within the range of 0.002−0.040 au", and "the corresponding Laplacian in the range from 0.024 to 0.139 au" seems to be one of the most important ones.[46] The values of $\rho(r)$ and $\nabla^2\rho(r)$ corresponding to the optimized geometry of **I** are found to be 0.024 and 0.080 for $O_{17}$−$H_{24}\cdots N_7$ IMHB and 0.023 and 0.082 for $O_{17}\cdots H_{24}$−$N_7$ IMHB in **III**, respectively. For the optimized geometry of **IV**, the same parameters amount to 0.037 and 0.106 for $O_{17}$−$H_{24}\cdots O_{25}$ $I_{er}$MHB and 0.04 and 0.093 for $O_{25}$−$H_{27}\cdots N_7$ $I_{er}$MHB, respectively [$\rho(r)$ and $\nabla^2\rho$(r) corresponding to the optimized geometry of **V** take the values 0.04 and 0.139 for $O_{17}\cdots H_{24}$−$O_{25}$ and 0.037 and 0.103 for $O_{25}\cdots H_{27}$−$N_7$, respectively]. Therefore, the presence H-bonding in the studied molecular systems is evidenced on the basis of Kock and Propelier[46] criteria also. At the same time, different values of $\rho(r)$ and $\nabla^2\rho(r)$ for the two $I_{er}$MHBs present in **IV** and **V** advocate that they are not equally strong.

***3.2.3. Potential Energy Surface (PES) of Hydrated Cluster of 4-HA.*** The PESs for the proton transfer reaction of 4-HA-$H_2O$ in the $S_0$ and $S_1$ states have been computed at the DFT/B3LYP/6-311++G(d,p) and TDDFT/B3LYP/6-311++G(d,p) levels, respectively. As seen in Figure 5, the PES for 4-HA−$H_2O$ represents a global minimum for structure **IV** on the $S_0$ surface, and the possibility of ground state proton transfer (GSPT) is discarded since for GSPT to occur a transition state (**TS2**) with high barrier (barrier height = 12.16 kcal/mol) has to be passed through. But the asymmetric double-well-type potential surface along the reaction coordinate (RC) for the $S_1$ state is observed with two minima for **IV*** and **V*** conformers. The deviation of the nature of the $S_1$ surface of 4-HA−$H_2O$ in comparison to that for isolated 4-HA (Figure 2) is noteworthy. Figure 5 shows that in the first excited state ($S_1$), the process of proton transfer is rendered practically barrierless through one water molecule, i.e., the spontaneous conversion **IV**→**V**. At the same time, the thermodynamic stabilities of structures **IV** and **V** are inverted as a result of $S_0$→$S_1$ transition. A direct comparison of the results of sections 3.1.4 and 3.2.3 clearly demonstrates the impossibility of intrinsic ESIPT reaction in 4-HA, while the significant reduction of the barrier height for ESPT reaction by a single water molecule suggests the occurrence of water-mediated PT as was reported experimentally.[24]

As displayed in Scheme 2, in the monohydrated structure 4-HA−$H_2O$, the labile $H_{24}$ proton attached initially to $O_{17}$ and hydrogen bonded to $O_{25}$ of the water molecule is transferred to $O_{25}$ with simultaneous translocation of the second proton $H_{27}$ from $O_{25}$ to $N_7$, i.e., a case of transfer of two protons. However, the issue of the presence of any high-energy intermediate along

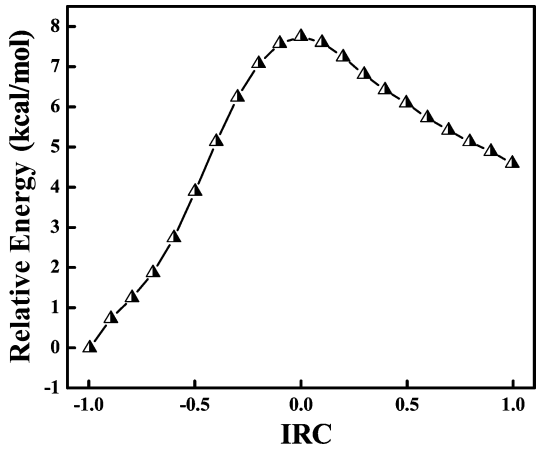


**Figure 6.** IRC for 4-hydroxyacridine water-assisted tautomerization **IV**→**V** calculated for the gaseous phase at the B3LYP/6-311++G(d,p) level.

the reaction path must be clarified at this point. Hence, we have calculated the IRC[19,29] for double proton transfer at the B3LYP/6-311++G(d,p) level and the result is portrayed in Figure 6, which conforms to the presence of no intermediate along IRC, suggesting smooth proceeding of the reaction from reactant to product. It is thus relevant to predict that it is a case of concerted and synchronous transfer of two protons.[19,20,29]

***3.2.4. Molecular Orbital Picture.*** The results obtained and hence the conclusion drawn from the analysis of the PESs for isolated 4-HA (section 3.1.4) and its monohydrated counterpart (4-HA−$H_2O$) (section 3.2.3) can further be afforded a supportive platform from the analysis of the molecular orbitals (HOMO and LUMO) along the proton transfer coordinate of the molecular system (DFT/B3LYP/6-311++G(d,p)). Nagaoka et al. in 1999 developed the nodal plane concept of the $\pi$-system molecular orbital to rationalize the phenomenon of ESIPT in 2-(*o*-hydroxyaryl)benzazoles[47] and latter extended the idea to a number of ESIPT systems to commendable fruition.[24,47−50] Here we apply the same concept in our case. Since the proton transfer has been observed in 4-HA−$H_2O$ only, the emphasis of the discussion in this section is entrusted on the HOMO−LUMO pictures of 4-HA−$H_2O$ only. But for a cogent visual comparison the MO diagrams of bare 4-HA are also provided (Figure 7a). As seen in Figure 7b, the HOMO of **IV** is an $\pi$ orbital composed of bonding contributions along $C_3-C_4-C_5$, $C_1-C_2$, and $N_7-C_{10}$ and a high electronic density projection over $O_{17}$. The antibonding contributions present along $C_4-O_{17}$, $C_5-N_7$ are also noteworthy. Similar characteristics are observed for the HOMO of structure **V** also, i.e., bonding character along $C_3-C_4-C_5$, $C_2-C_1-C_6$, and $N_7-C_{10}$ along with antibonding contributions across $C_4-O_{17}$ and $C_5-N_7$. In addition, the electronic density projection on $O_{17}$ for **V** is somewhat greater than that in **IV**. The HOMO of both **IV** and **V** shows large electronic density projection over $O_{17}$ with bonding character along $N_7-C_{10}$. This indicates that transfer of proton in the ground state leads to no further stabilization through electronic redistribution.

The LUMO is an $\pi^*$ type orbital for both structures **IV** and **V**. In the LUMO of **IV**, large bonding contributions across $C_1-C_6-C_5-C_4$ and $C_{14}-C_9-C_{10}-C_{11}$ are observed, with simultaneous antibonding character along $C_5-N_7$ and $N_7-C_{10}$. Similar characteristics for LUMO of **V** are observed. However, for the HOMO→LUMO transition for both **IV** and **V**, a relative decrement of electronic density projection over $O_{17}$ is noticed. The presence of antibonding contributions in the LUMO across $C_4-O_{17}$, $N_7-C_{10}$, and $C_5-N_7$ is crucial, since it prevents electronic delocalization in the aromatic nucleus, thereby preventing the reversal of PT in the excited state. Also excitation of electron from HOMO to LUMO associates noteworthy rearrangement of electronic density, particularly across the $I_{er}$MHB system.

**3.3. Structure and Potential Energy Surface of Hydrated Cluster of 4-HA with Two Water Molecules.** Foregoing discussions reveal that the process of ESPT in 4-HA is considerably more favorable when it is assisted via the mediacy of one water molecule compared to that in bare 4-HA. An intrinsic ESIPT process in bare 4-HA encounters a barrier height of 5.50 kcal/mol on the $S_1$ surface (Figure 2), while it is rendered practically barrierless for 4-HA monohydrated cluster (Figure 5). Thus, it is pertinent to find out the optimum number of water molecules with which the process of ESPT in 4-HA would be most efficient. With a view to implement the search, we have looked for the possibility of a two-water-molecule-mediated PT reaction in 4-HA. Here we have optimized the geometries of the enol (**VI**) and keto (**VII**) forms of 4-HA clustered with two water molecules and the corresponding transition state (**TS3**) at the DFT/B3LYP/6-311++G** level of theory. Schematics of structures of **VI**, **VII**, and **TS3** are presented in Scheme 3.

From the schematic diagram of PT reaction (Figure 8) representing the transformation **VI**→**VII**, it is evident that the barrier for the transformation on the $S_1$ surface is 4.13 kcal/mol, which is smaller than the barrier in the case of isolated 4-HA molecule (5.5 kcal/mol for transformation **I**→**III**) but much higher than that in the case of one water cluster of 4-HA. In the ground state PES, both the calculated forward and backward energy barriers are quite high (16.66 and 11.87 kcal/mol, respectively). These results evidence that the barrier to ESPT reaction in 4-HA in the $S_1$ excited state attains its minimum value for one water cluster of 4-HA while for the two-water cluster it again rises.

## 4. Conclusion

In this paper, we have studied the IMHB formation, excited state proton transfer reaction, and charge distribution in 4-HA in the gaseous phase and in solution using the DFT method. Two SCRF models have been implemented to account for solvent effects. The marked instability of the proton transferred form (conformer **III**) with respect to the normal form (conformer **I**) in the ground state in the gaseous phase is connected to the extra stability due to IMHB in the latter, whereas a reversal of the stability pattern in solvent water shows a clear sign of preferable stabilization of the more polar entity. These results also advocate the profound influence of solvent reaction field on the concerned structures. In the excited state surface, the proton transfer forms are found to be more stable than the corresponding normal form in all cases of bare molecules and its hydrates. NBO analysis also revealed their potential in exploring the nature of bonds in the complexes. It is found that the strongest intermolecular interaction involving charge transfer from $O_{17}$ to the antibonding $\sigma^*(O_{25}-H_{24})$ takes place in aqueous solution, a manifestation of which is found in the relatively high occupation number of the antibond. The changes in geometric parameters brought about by the action of the solvent have also been studied in light of NBO analysis. The nature of H-bonds has been explored within the AIM framework for 4-HA and its monohydrate in terms of the calculated $\rho(r)$ and Laplacian $\nabla^2\rho(r)$ at the bond critical point (BCP).

Calculations predict the high-energy barrier in the forward proton transfer reaction in 4-HA and its mono- and dihydrates in the ground state. But for the reverse direction the calculated

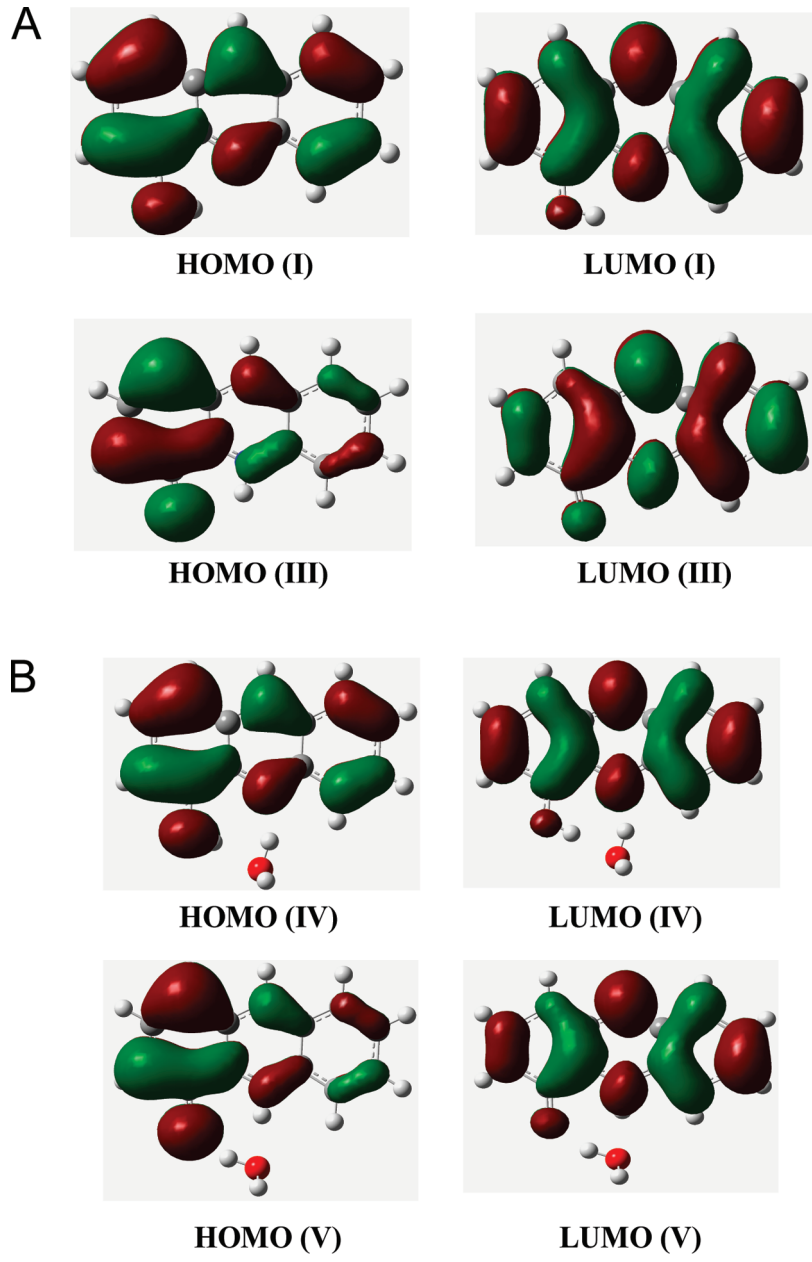


**Figure 7.** Two-dimensional plots of the HOMO and LUMO orbitals (as obtained with DFT/B3LYP/6-311++G(d,p)) that are involved in the electronic excitation from $S_0$ to $S_1$ of conformers (a) **I** and **III** and (b) **IV** and **V**.

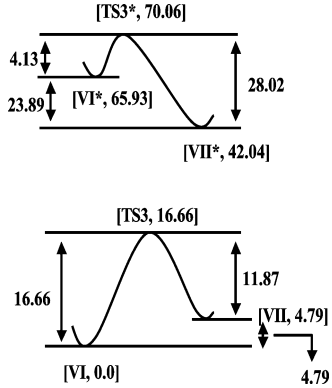


**Figure 8.** Schematic of PES for transformation **VI**→**VII** at the DFT//B3LYP/6-311++G(d,p) level (Energies in kcal/mol).

barrier is comparatively low. This dictates the impracticability of the GSPT process. In the singlet excited surface ($S_1$ state), the barriers for proton transfer reaction are respectively 5.5 and 4.13 kcal/mol in the case of 4-HA and its dihydrated cluster. But as soon as a single water molecule comes to play by bridging between the donor and acceptor sites of 4-HA, the process of PT is rendered essentially barrierless, i.e., the signature of the phenomenon of water-mediated proton transfer. That the double-proton transfer in water-assisted tautomerization of 4-HA−$H_2O$ occurs via a concerted and synchronous pathway is also predicted from our calculations (no intermediate along IRC). Furthermore, MO pictures are in line with the conclusions drawn from PESs of 4-HA−$H_2O$.

**Acknowledgment.** N.G. acknowledges CSIR, India (Project no. 01(2161)07/EMR-II) and DST, India (Project no. SR/S1/PC/26/2008) for financial support. B.K.P. is grateful to CSIR, New Delhi, India for research fellowship.

## References and Notes


(1) (a) Morris, D. R.; Hager, L. P. *J. Biol. Chem.* **1966**, *241*, 3582. (b) Taurog, A. *Endocrinology* **1976**, *98*, 1031. (c) Engler, H.; Taurog, A.; Nakashima, T. *Biochem. Pharmacol.* **1982**, *31*, 3801. (d) Ahren, B.; Rerup, C. *Pharmacol. Toxicol.* **1987**, *61*, 69. (e) Lindsay, H. R.; Cash, A. G.; Vaugh, A. W.; Hill, J. B. *Biochem. Pharmacol.* **1977**, *26*, 617. (f) Bjorstein, F. *Biochim. Biophys. Acta* **1966**, *127*, 265.

(2) Gonzalez, V. M.; Fuertes, M. A.; Perez-Alvarez, M. J.; Cervantes, G.; Moreno, V.; Alonso, C.; Perez, J. M. *Biochem. Pharmacol.* **2000**, *60*, 371.

(3) Aziz, S. A.; Knowles, C. O. *Nature* **1973**, *242*, 418.

(4) Beeman, R. W.; Matsumura, F. *Nature* **1973**, *242*, 274.

(5) Johnson, T. L.; Knowles, C. O. *Gen. Pharm* **1983**, *14*, 591.

(6) Silverman, D. N.; Lindslog, S. *Acc. Chem. Res.* **1988**, *21*, 30.

(7) Jasien, P. G.; Stevens, W. J. *J. Chem. Phys.* **1986**, *84*, 3271.

(8) Bell, R. L.; Truong, T. N. *J. Chem. Phys.* **1994**, *101*, 10442.

(9) Yamabe, S.; Tsuchida, N.; Hayashida, Y. *J. Phys. Chem. A* **2005**, *109*, 7216.

(10) Tortonda, F. R.; Pascul-Ahuir, J. L.; Silica, E.; Tunon, I. *Chem. Phys. Lett.* **1996**, *260*, 21.

(11) Markova, N.; Enchev, V.; Timtchera, I. *J. Phys. Chem. A.* **2005**, *109*, 1981.

(12) Dkhissi, A.; Adamowick, L.; Maes, G. *Chem. Phys. Lett.* **2000**, *324*, 127.

(13) Kim, Y.; Lim, S.; Kim, H.-J.; Kim, Y. *J. Phys. Chem.* **1999**, *103*, 617.

(14) Tsuchida, N.; Yambe, S. *J. Phys. Chem.* **2005**, *109*, 1974.

(15) Li, Q.-S.; Fang, W.-H. *Chem. Phys. Lett.* **2003**, *367*, 637.

(16) Wang, X.-C.; Nichols, J.; Feyereisen, M.; Gutowski, M.; Boatz, J.; Haymet, J. A. D.; Simons, J. *J. Phys. Chem.* **1991**, *95*, 10419.

(17) Bell, R. L.; Taveras, D. L.; Truong, T. N.; Simons, *Int. J. Quantum Chem.* **1997**, *63*, 861.

(18) Catalan, J.; Perez, P.; del Valle, J. C.; de Paz, J. L. G.; Kasha, M. *Proc. Natl. Acad. Sci. U.S.A.* **2004**, *101*, 419.

(19) Hazra, M.; Chakraborty, T. *J. Phys. Chem. A* **2005**, *109*, 7621.

(20) Hazra, M.; Chakraborty, T. *J. Phys. Chem. A* **2006**, *110*, 9130.

(21) Podolyan, Y.; Gorb, L.; Leszcynski, J. *J. Phys. Chem. A* **2002**, *106*, 12130.

(22) Gordon, M. S. *J. Phys. Chem.* **1996**, *110*, 3974.

(23) Sobolewski, A. L.; Domcke, W.; Hättig, C. *Proc. Natl. Acad. Sci. U.S.A.* **2005**, *102*, 17903.

(24) Singh, R. B.; Mahanta, S.; Guchhait, N. *J. Photochem. Photobiol. A: Chem.* **2008**, *200*, 325.

(25) Hung, F.-T.; Hu, W.-P.; Li, T.-H.; Cheng, C.-C.; Chou, P.-T. *J. Phys. Chem. A.* **2003**, *107*, 3244.

(26) Sawicki, E.; McPherson, S. P.; Stanley, T. W. *Int. J. Air Water Pollut.* **1965**, *9*, 515.

(27) Pucci, D.; Albertini, V.; Bloise, R.; Bellusci, A.; Cataldi, A.; Catapano, C. V.; Ghedini, M.; Crispini, A. *J. Inorg. Biochem.* **2006**, *100*, 1775.

(28) (a) Foresman, J. B.Æ.; FrischM. J. *Exploring Chemistry with Electronic Structure Methods*, 2nd ed.; Gaussian, Inc.: Pittsburgh, PA, 1996. (b) Frisch, M. J. et. al. *Gaussian 03*; Gaussian, Inc.: Pittsburgh, PA, 2003.

(29) Shchavlev, A. E.; Pankratov, A. N.; Shalabay, A. V. *J. Phys. Chem. A* **2005**, *109*, 4137.

(30) Hehre, W. J.; Radom, L.; Schleyer, P. v.; Pople, J. A. *Ab Initio Molecular Orbital Theory*; Wiley: New York, 1986.

(31) Foresman, J. B.; Frisch, A. *Exploring Chemistry with Electronic Structure Methods*, 2nd ed.; Gaussian, Inc.: Pittsburgh, PA, 1996.

(32) Clark, T.; Chandrasekhar, J.; Spitznagel, G. W.; Schleyer, P. v. R. *J. Comput. Chem.* **1983**, *4*, 294.

(33) Onsager, L. *J. Am. Chem. Soc.* **1936**, *58*, 1486.

(34) Cossi, M.; Barone, V.; Mennucci, B.; Tomasi, J. *Chem. Phys. Lett.* **1998**, *286*, 253.

(35) Mennucci, B.; Tomasi, J. *J. Chem. Phys.* **1997**, *106*, 5151.

(36) Boys, S. F.; Bernadi, F. *Mol. Phys.* **1970**, *19*, 553.

(37) Schlegel, H. B. *J. Comput. Chem.* **2003**, *24*, 1514.

(38) Ayala, P. Y.; Schlegel, H. B. *J. Chem. Phys.* **1997**, *107*, 375.

(39) (a) Reed, A. E.; Curtiss, L. A.; Weinhold, F. A. *Chem. Rev.* **1988**, *88*, 899. (b) Glendening, E. D.; Reed, A. E.; Carpenter, J. E.; Weinhold, F. A. *NBO, Version 3.1*, 1995.

(40) Hobza, P.; Havlas, Z. *Chem. Rev.* **2000**, *100*, 4253.

(41) (a) Galvez, O.; Gomez, P. C.; Pacios, L. F. *J. Chem. Phys.* **2001**, *115*, 11166. (b) Galvez, O.; Gomez, P. C.; Pacios, L. F. *J. Chem. Phys.* **2003**, *118*, 4878. (c) Woodford, J. N. *J. Phys. Chem. A* **2007**, *111*, 8519.

(42) Casida, M. E.; Jamorski, C.; Casida, K. C.; Salahub, D. R. *J. Chem. Phys.* **1998**, *108*, 4439.

(43) Stratmann, R. E.; Scuseria, G. E.; Frisch, M. J. *J. Chem. Phys.* **1998**, *109*, 8218.

(44) (a) Maheshwary, S.; Chowdhury, A.; Sathyamurthy, N.; Mishra, H.; Tripathi, H. B.; Panda, M.; Chandrasekhar, J. *J. Phys. Chem. A* **1999**, *103*, 6257. (b) de Vivie-Riedle, R.; Waele, V. D.; Kurtz, L.; Riedle, E. *J. Phys. Chem. A* **2003**, *107*, 10591.

(45) (a) Marechel, Y. *The Hydrogen Bond And the Water Molecule: The Physics And Chemistry of Water, Aqueous and Bio-media*; Elsevier Science Ltd.: Amsterdam, 2006. (b) Jeffrey, G. A. *An Introduction to Hydrogen Bonding*; Oxford University Press: New York, 1997.

(46) (a) Koch, U.; Popelier, P. L. A. *J. Phys. Chem.* **1995**, *99*, 9747. (b) Popelier, P. L. A. *J. Phys. Chem. A* **1998**, *102*, 1873.

(47) (a) Nagaoka, S.; Nagashima, U. *Chem. Phys.* **1996**, *206*, 353. (b) Nagaoka, S.; Kusunoki, J.; Fujibuchi, T.; Hatakenaka, S.; Mukai, K.; Nagashima, U. *J. Photochem. Photobiol. A: Chem.* **1999**, *122*, 151. (c) Nagaoka, S.; Nakamura, A.; Nagashima, U. *J. Photochem. Photobiol. A: Chem.* **2002**, *154*, 23.

(48) Catalan, J.; de Paz, J. L. G. *J. Phys. Chem. A* **2007**, *112*, 904.

(49) Amati, M.; Belviso, S.; Cristinziano, P. L.; Minichino, C.; Lelj, F.; Aiello, I.; Deda, M. L.; Chedini, M. *J. Phys. Chem. A* **2007**, *111*, 13403.

(50) Singh, R. B.; Mahanata, S.; Guchhait, N. *Chem. Phys.* **2007**, *331*, 189.


JP909029C